Anatomy of octupole correlations in ^{96}Zr with a symmetry-restored multidimensionally-constrained covariant density functional theory

Yu-Ting Rong [a,b], Xian-Ye Wu [c], Bing-Nan Lu [d,*], Jiang-Ming Yao [e]

[a] *Department of Physics, Guangxi Normal University, Guilin, 541004, China*
[b] *CAS Key Laboratory of Theoretical Physics, Institute of Theoretical Physics, Chinese Academy of Sciences, Beijing, 100190, China*
[c] *College of Physics and Communication Electronics, Jiangxi Normal University, Nanchang, 330022, China*
[d] *Graduate School of China Academy of Engineering Physics, Beijing, 100193, China*
[e] *School of Physics and Astronomy, Sun Yat-sen University, Zhuhai, 519082, China*

A B S T R A C T

A recent analysis based on the STAR measurement in relativistic heavy-ion collision experiments provides evidence of octupole correlation in the ground state of ^{96}Zr, the description of which presents a challenge to nuclear structure models. In this work, we perform projection-after-variation calculations for ^{96}Zr based on a multidimensionally-constrained relativistic Hartree-Bogoliubov model. Our results show that an octupole deformed shape is favored in energy after symmetry restoration, and this phenomenon cannot be reproduced in the pure mean-field calculations. These complex structures originate from the competition among various shell structures in this mass region. Our results suggest that the allowance of symmetry breaking at the mean-field level and the restoration of broken symmetries are essential elements for understanding the structure of ^{96}Zr in density functional theories.

1. Introduction

In atomic nuclei, the occurrence of spontaneous symmetry breaking results in various shapes. The most common nuclear shape is the ellipsoid. For some specific proton or neutron numbers, we can also find pronounced pear-like shapes [1–6]. For a long time, the only reliable method for studying these reflection-asymmetric shapes has been to search for the characteristic patterns of parity and angular momentum in nuclear spectroscopy. For example, the enhanced reduced electric-octupole transition probabilities, $B(E3)$, in ^{224}Ra [7], ^{144}Ba [8], ^{146}Ba [9], and ^{228}Th [10] can be viewed as direct experimental evidences of strong octupole deformations.

Recently, it has been proposed that nuclear deformations can also be extracted from relativistic heavy-ion collisions (RHIC) by analysing the hydrodynamic collective flow of the final-state particles [11–15]. Later this method was applied to study realistic experimental data [16–19]. In Ref. [20], the deformations of ^{96}Zr and ^{96}Ru were extracted from isobaric ^{96}Zr+^{96}Zr and ^{96}Ru+^{96}Ru collisions, respectively. By analyzing the elliptic flow v_2 and triangular flow v_3 [21], the authors inferred a strong octupole deformation in ^{96}Zr and a strong quadrupole deformation in ^{96}Ru.

The onset of large octupole correlation in the low-lying states of atomic nuclei is attributed to the existence of pairs of single-particle orbitals with opposite parities strongly coupled by the octupole moments near the Fermi level [1]. Consequently, nuclei with neutron or proton numbers near the octupole magic numbers 34, 56, 88, and 134 are natural candidates for searching for the pear-like nucleus. ^{96}Zr, whose neutron number is $N = 56$, is one of these nuclei and expected to show reflection-asymmetric shapes [22–29]. The experimentally observed large $B(E3)$ value in its ground-state band indicates a strong octupole collectivity [22–25,29], which is also corroborated by recent RHIC experiments [20]. Conversely, all systematic search for the octupole deformations based on modern nuclear structure theories, including the macroscopic-microscopic (MM) model [30], the relativistic Hartree-Bogoliubov (RHB) theory [5], the Hartree-Fock-Bogoliubov (HFB) theories with Gogny interaction [4] and Skyrme interactions [6], do not find any octupole deformation for ^{96}Zr. Instead, all these theoretical investigations except for the MM model find octupole deformations near $N = Z = 40$, which is incompatible with both the experiments and the argument of octupole magic numbers. To reconcile this inconsistency between the theories and experiments, we need to consider the beyond-mean-field effects not included in the systematic calculations.

* Corresponding author.
E-mail address: bnlv@gscaep.ac.cn (B.-N. Lu).

Doctopic: Theory

ARTICLE IN PRESS

JID:PLB   AID:137896 /SCO

[m5G; v1.335] P.2 (1-7)

Y.-T. Rong, X.-Y. Wu, B.-N. Lu et al.

Physics Letters B ••• (••••) ••••••

The nuclear density functional theories are very successful in describing the nuclear deformations microscopically. In these calculations, the ground states are obtained by applying the variational principle with a Slater determinant or a Bogoliubov vacuum. The resulting states usually violate fundamental symmetries and conservation laws, such as rotational symmetry, translational invariance and particle-number conservation [31]. As a consequence, projection-after-variation (PAV) techniques are employed to restore the broken symmetries and calculate observables with good quantum numbers [32–37]. PAV calculations have been applied to study the octupole deformations in Ra isotopes based on shell model wave functions [38], in Ra isotopes [39] and ^{20}Ne [40] based on Dirac wave functions, in Ba, Ra isotopes [41,42], Zr isotopes [43], ^{16}O [44], actinides, superheavies [45] and other nuclei [46] based on HFB wave functions. There are also theoretical investigations of octupole deformations based on the multidimensional collective Hamiltonian [47,48] and the interacting boson model [49]. The octupole deformations in Zr isotopes have been discussed using the generator-coordinate method (GCM) with a partial angular momentum [28] or parity [50,51] projection. Besides the axial deformations, recent PAV calculations based on Gogny interaction predicted a tetrahedral shape associated with a pure non-axial β_{32} deformation in ^{96}Zr [43]. Nevertheless, so far there is no systematic investigations for the evolution of octupole deformations in the $A \sim 100$ region based on full angular momentum and parity projections. Such calculations will provide necessary knowledge that can help understand the recent RHIC experiments as well as the spectroscopic data.

For studying the various nuclear shapes in a unified framework, the multidimensionally-constrained relativistic Hartree-Bogoliubov (MDCRHB) model has been developed, in which both the axial and spatial reflection symmetries are broken but the simplex symmetry is preserved [52,53]. Recently we developed a projected multidimensionally-constrained relativistic Hartree-Bogoliubov (p-MDCRHB) model by incorporating the parity and angular momentum projections into the MDCRHB model to study the low-lying states related to exotic nuclear shapes, e.g., the triangular shape associated with the three-α configuration in ^{12}C [54].

In this paper, we investigate the octupole correlations in ^{96}Zr by employing the p-MDCRHB model. We present a systematic beyond-mean-field study with both triaxial and octupole shapes included simultaneously. In Sec. 2, the theoretical framework of this model is introduced. In Sec. 3, we use the p-MDCRHB model to calculate the projected PESs in ^{96}Zr and extract the deformations and excitation energies of the low-lying states. The results are discussed in comparison with spectroscopic measurements and relativistic collision experiments. The microscopic mechanism of the octupole correlations are analyzed based on the evolution of single-particle shell structures. Finally, a summary is given in Sec. 4.

2. Theoretical framework

We start with the RHB theory with effective point coupling interactions [55,56]. The RHB equation in coordinate space reads [57,58]

$$\int d^3\mathbf{r}' \begin{pmatrix} h-\lambda & \Delta \\ -\Delta^* & -h+\lambda \end{pmatrix} \begin{pmatrix} U_k \\ V_k \end{pmatrix} = E_k \begin{pmatrix} U_k \\ V_k \end{pmatrix}, \tag{1}$$

where Δ is the pairing field, λ is the Fermi energy, E_k is the quasi-particle energy and $(U_k(\mathbf{r}), V_k(\mathbf{r}))^T$ is the quasi-particle wave function. h is the single-particle Hamiltonian,

$$h = \boldsymbol{\alpha} \cdot \mathbf{p} + \beta[M + S(\mathbf{r})] + V(\mathbf{r}), \tag{2}$$

where M is the nucleon mass, $S(\mathbf{r})$ is the scalar potential, and $V(\mathbf{r})$ is the vector potential. In this work, we use the PC-PK1 parameter

set [59] and solve the RHB equation by expanding the wave functions on an axially-deformed harmonic oscillator basis. For pairing interaction, we adopt a separable pairing force of finite range in the spin-singlet channel [60,61],

$$V = -G\delta(\mathbf{R} - \mathbf{R}')P(\mathbf{r})P(\mathbf{r}')\frac{1 - P_\sigma}{2}, \tag{3}$$

where G is the pairing strength, $\mathbf{R} = (\mathbf{r}_1 + \mathbf{r}_2)/2$ and $\mathbf{r} = \mathbf{r}_1 - \mathbf{r}_2$ are the center of mass and relative coordinates, respectively. The symbols with and without the prime denote the quantities before and after the interaction, respectively. P_σ is the spin-exchange operator. $P(\mathbf{r}) = (4\pi a^2)^{-3/2}e^{-r^2/4a^2}$ is the Gaussian function. $a = 0.644$ fm is the effective range of the pairing force. In this work we use different pairing strength for neutron and proton, $G_n = 728.00$ MeV·fm^3 and $G_p = 815.36$ MeV·fm^3. These parameters were adjusted to reproduce the available empirical pairing gaps of ^{102,104}Zr [62].

Nuclear shapes are characterized by the deformation parameters $\beta_{\lambda\mu}$ which are defined as

$$\beta_{\lambda\mu} = \frac{4\pi}{3AR^\lambda}Q_{\lambda\mu}, \tag{4}$$

where $R = 1.2A^{1/3}$ fm with A the mass number, $Q_{\lambda\mu}$ is the multipole moment of the intrinsic densities. With symmetry imposed in this model, all $\beta_{\lambda\mu}$ with even μ can be considered simultaneously.

In the p-MDCRHB model [54], the nuclear wave function $|\Phi(q)\rangle$ is projected onto the parity π and angular momentum J

$$|\Psi_{\alpha,q}^{JM\pi}\rangle = \sum_K f_\alpha^{JK\pi} \hat{P}_{MK}^J \hat{P}^\pi |\Phi(q)\rangle, \tag{5}$$

where $f_\alpha^{JK\pi}$ is the weight function, q represents a collection of the deformation parameters,

$$\hat{P}_{MK}^J = \frac{2J+1}{8\pi^2}\int d\Omega D_{MK}^{J*}(\Omega)\hat{R}(\Omega) \tag{6}$$

is an operator which projects out the component with angular momentum J and its projection M from the deformed mean-field wave function. K is angular momentum projection onto z-axis in the intrinsic frame. $D_{MK}^J(\Omega)$ is the Wigner function with a Euler angle $\Omega \equiv \{\phi, \theta, \psi\}$. $\hat{R}$ represents spatial rotation. The parity projection operator writes

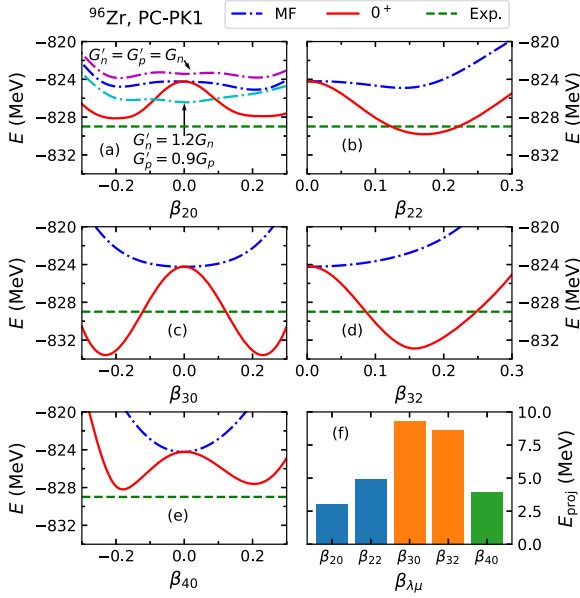$$\hat{P}^\pi = \frac{1}{2}(1 + \pi\hat{P}), \tag{7}$$

where $\hat{P}$ is the spatial reflection operation.

Considering that the projection calculation with both rotational and parity symmetry breaking is already costly, in this first step towards full projection, we do not include the exact particle number projection. Instead, we add two correction terms to the Hamiltonian kernel as in Ref. [63] to approximately restore the average proton and neutron numbers, i.e.,

$$\mathcal{H}' = \mathcal{H} - \lambda_p[Z(\mathbf{r}; q, q'; \Omega) - Z_0] - \lambda_n[N(\mathbf{r}; q, q'; \Omega) - N_0], \tag{8}$$

where λ_p and λ_n are the Fermi energies for protons and neutrons of the mean-field state $|\Phi(q)\rangle$, $Z(\mathbf{r}; q, q'; \Omega)$ and $N(\mathbf{r}; q, q'; \Omega)$ are the mixed vector densities for protons and neutrons, respectively. Z_0 and N_0 are the target proton and neutron numbers, respectively. After calculating the mixed energy density, the weight function $f_\alpha^{JK\pi}$ and the eigenvalue $E_\alpha^{J\pi}$ are obtained by solving the generalized eigenvalue equation in the standard way [64,65]:

$$\sum_{K'}\left\{\mathcal{H}_{KK'}'^{J\pi}(q;q) - E_\alpha^{J\pi}\mathcal{N}_{KK'}^{J\pi}(q;q)\right\}f_\alpha^{JK'\pi} = 0, \tag{9}$$

Doctopic: Theory

ARTICLE IN PRESS

JID:PLB   AID:137896 /SCO   [m5G; v1.335] P.3 (1-7)

Y.-T. Rong, X.-Y. Wu, B.-N. Lu et al.   Physics Letters B ••• (••••) ••••••

Fig. 1. The one-dimensional mean-field (dash-dotted lines) and projected 0^+ (solid lines) potential energy surfaces of ^{96}Zr with pure β_{20} (a), β_{22} (b), β_{30} (c), β_{32} (d) and β_{40} (e) deformations, and projection energy as a function of $\beta_{\lambda\mu}$ (f). If not specified on the figure, the pairing strengths are $G_p = 815.36$ MeV·fm^3 and $G_n = 728.00$ MeV·fm^3. The experimental binding energy $E = -828.99$ MeV [74] is shown as dashed line.

where $\mathcal{N}$ is the norm kernel. To check the validity of the ansatz of introducing the correction terms in Eq. (8), we also carry out a beyond relativistic mean-field calculation with exact particle-number projections by employing the approach developed in Ref. [39].

We note that the restoration of broken symmetries with modern nuclear energy density functionals usually meet the problems of spurious divergencies [66,67] and finite steps [68–71]. The solution to this problem in a proper way is still an open question. Of course, these issues can be avoided in Hamiltonian-based frameworks if all the terms in the projected energy are taken into account in a consistent way, in particular Fock terms and contributions of the Coulomb and spin-orbit potentials to pairing, etc. [66,72,73]. In the current covariant density functional theories, these problems remain in one way or another. They are not serious in this work as the symmetry restoration is carried out after variation. Besides, to avoid the numerical ambiguity from the division of zero by zero, an odd number of mesh points in the integration over the gauge angles for particle number projection is adopted. More arguments have already been made in Ref. [65].

3. Results and discussions

In MDCRHB model and its extensions, thanks to the usage of an unified axial symmetric basis, we can alleviate the computational burden by simply disregarding the matrix elements that violate the specific symmetries. We break a symmetry if and only if it is an essential element in describing certain processes we are focusing on. Therefore, four types of spatial symmetries can be imposed and associated with some non-zero quadrupole-octupole deformations: (a) axial-reflection symmetry with only β_{20}; (b) non-axial but reflection symmetry with (β_{20}, β_{22}); (c) axial symmetry but reflection asymmetry with (β_{20}, β_{30}); (d) non-axial and reflection asymmetry with $(\beta_{20}, \beta_{22}, \beta_{30}, \beta_{32})$, which are labeled as $K\pi$, $\not{K}\pi$, $K\not{\pi}$, and $\not{K}\not{\pi}$, respectively.

Fig. 1(a-e) shows the total energy of ^{96}Zr as a function of β_{20}, β_{22}, β_{30}, β_{32} and β_{40}, respectively, where all other deformation parameters are constrained to be zero. The dash-dotted and solid

lines correspond to the mean-field and projected 0^+ PESs, respectively. It is shown in Fig. 1(a) that the mean-field energy surface is very soft around the spherical shape. Any slight changes of the pairing strength may shift the location of the energy minimum. Specifically, with $G_n = 728.00$ MeV·fm^3 and $G_p = 815.36$ MeV·fm^3, we obtain two energy minima located at prolate ($\beta_{20} = 0.21$) and oblate ($\beta_{20} = -0.19$) respectively with energy difference 0.32 MeV. If we enhance (quench) the neutron (proton) pairing strength by 20%(10%), the PES is still soft, but the energy minimum is shifted to the spherical shape. A proper description of the ground state needs to go beyond the mean-field approximation.

For $E(\beta_{22})$ shown in Fig. 1(b), the mean-field PES is very soft. The projected 0^+ energy minimum is located at $\beta_{22} = 0.17$ and the corresponding binding energy is slightly overestimated. The PESs $E(\beta_{30})$ and $E(\beta_{32})$ with octupole deformations are shown in Fig. 1(c) and (d). One can see that the energy minimum in the mean-field PES is shifted from spherical to octupole deformed state with $\beta_{30} = 0.23$ or $\beta_{32} = 0.16$ respectively after symmetry restorations. The energies gained from projection are 9.33 MeV and 8.65 MeV, respectively, which are consistent with the results of HFB model with Gogny interaction [43]. For $E(\beta_{40})$ in Fig. 1(e), The energy minimum changes from spherical to hexadecapole shape after projections and we gain 3.9 MeV extra binding energy by symmetry restorations. We define the projection energy E_{proj} as

$$E_{\text{proj}} = E(\text{MF})_{\text{min}} - E(0^+)_{\text{min}}, \qquad (10)$$

where $E(\text{MF})_{\text{min}}$ and $E(0^+)_{\text{min}}$ are the global energy minima on the mean-field and 0^+ PESs under the same symmetry restriction respectively, and show them in Fig. 1(f). One can find E_{proj}'s for octupole deformations are the dominant ones, which are larger than those for quadrupole and hexadecapole deformations.

Next we turn to the two-dimensional PESs. The results are shown in Fig. 2. We also list the deformation $\beta_{\lambda\mu}$, projection energy E_{proj} and excitation energy E_x corresponding to the global energy minima E_{min} on each PES in Table 1. We define E_x as
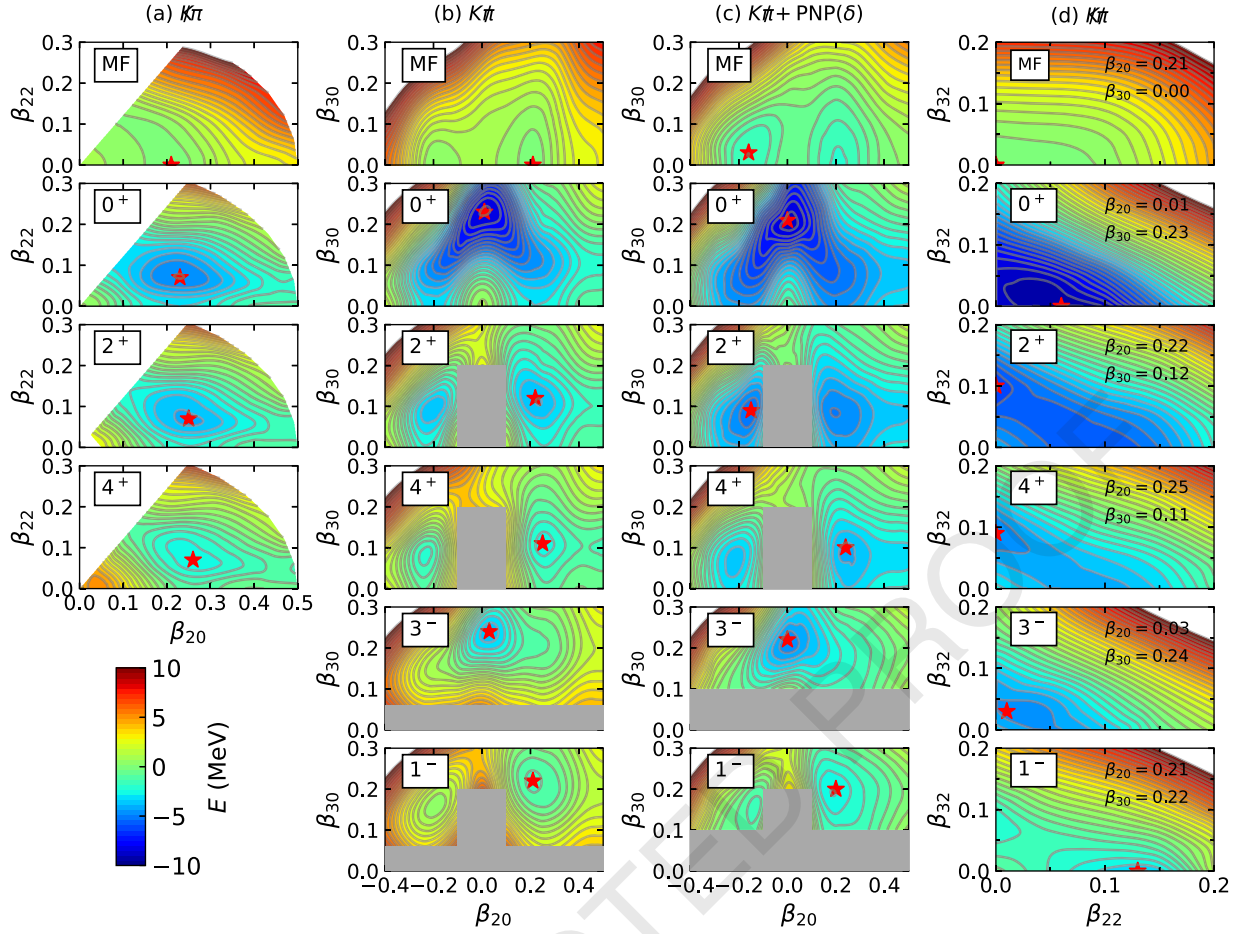
$$E_x(J^\pi) = E(J^\pi)_{\text{min}} - E(0^+)_{\text{min}}, \qquad (11)$$

where we compare the energy minima on different PESs which usually take different shapes. Note that this approximation only works for states with definite shapes. For soft PESs we also need the GCM to take into account the shape fluctuations or shape coexistence.

In $K\pi$ calculations, thanks to the six-fold symmetry with pure quadrupole deformations, we constrain the Hill-Wheeler coordinates $\beta_2 = \sqrt{\beta_{20}^2 + 2\beta_{22}^2}$, $\gamma = \arctan(\sqrt{2}\beta_{22}/\beta_{20})$ with $\gamma \in [0, 60°]$ instead of (β_{20}, β_{22}). Note that the octupole deformations will spoil the elegant six-fold symmetry and we constrain $\beta_{\lambda\mu}$'s directly in other cases. The mean-field PES is soft along the γ direction and the two energy minima correspond to the prolate and oblate shape isomers in Fig. 1(a), respectively. After symmetry projections, there is only one energy minimum with $(\beta_{20}, \beta_{22}) = (0.23, 0.07)$, i.e., $(\beta_2, \gamma) = (0.25, 23°)$ in Hill-Wheeler coordinates. Thus the ground state of ^{96}Zr is triaxially deformed, consistent with the Monte Carlo shell-model (MCSM) calculations [76]. The triaxial degree of freedom also appears in the energy minima of the 2^+ and 4^+ PESs. These energy minima assume similar deformations, indicating that they belong to the same collective band. The excitation energies $E_x(2^+) = 0.91$ MeV and $E_x(4^+) = 2.31$ MeV are lower than their corresponding experimental values 1.75 MeV and 2.75 MeV [75], respectively.

In Fig. 2(b) we present the mean-field and projected PESs $E(\beta_{20}, \beta_{30})$ with the $K\not{\pi}$ symmetries. On the mean-field PES, the two energy minima are located in $(\beta_{20}, \beta_{30}) = (0.21, 0.00)$ and

Doctopic: Theory
ARTICLE IN PRESS
JID:PLB AID:137896 /SCO
[m5G; v1.335] P.4 (1-7)
Y.-T. Rong, X.-Y. Wu, B.-N. Lu et al.
Physics Letters B ••• (••••) ••••••

Fig. 2. The two-dimensional mean-field (MF), $J^{\pi} = 0^+, 2^+, 4^+, 1^-$ and 3^- potential energy surfaces with (a) $\cancel{K}\pi$, (b) $K\cancel{\pi}$, and (d) $\cancel{K}\cancel{\pi}$ symmetry imposed. The (c) $K\cancel{\pi}$+PNP(δ) case calculated by using three-dimensional harmonic oscillator expansion method and density-dependent δ pairing force developed in Ref. [39] are shown for comparison. The contours join points with the same energy, and the separation between adjacent contours is 0.5 MeV. On each PES the red star marks the corresponding global energy minima. The values marked in (d) are the constrained (β_{20}, β_{30}) in this column, which are found in the global minima of (b). In each column the energies are relative to the mean-field ground state.
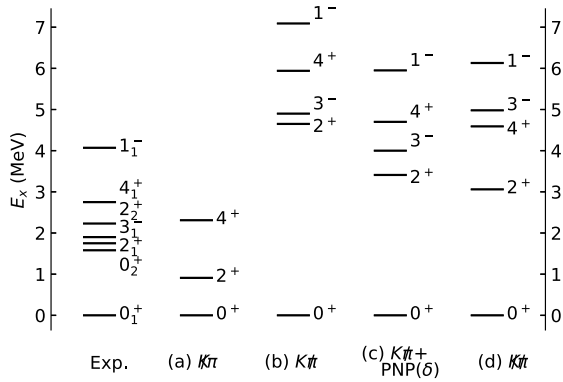
Table 1
The deformations $\beta_{\lambda\mu}$ and excitation (projection) energies E_x (E_{proj}) of various J^{π} (MF) states for ^{96}Zr. $E(0^+)_{min}$ denote the energy of the projected 0^+ states. All excitation energies are relative to the 0^+ states with the same symmetry. For $\cancel{K}\cancel{\pi}$ symmetry, (β_{20}, β_{30}) deformations are the same as those in the $K\cancel{\pi}$ global energy minimum. In the last line, the deformations inferred from the RHIC experiments [20] are listed for comparison. The experimental excitation energies are taken from Ref. [75]. All energies are in MeV.

Sym.	(a) $\cancel{K}\pi$			(b) $K\cancel{\pi}$			(c) $K\cancel{\pi}$+PNP(δ)			(d) $\cancel{K}\cancel{\pi}$			Exp.
$E(0^+)_{min}$	-829.978			-833.616			-832.329			-834.546			-828.99
State	β_{20}	β_{22}	$E_{x/proj}$	β_{20}	β_{30}	$E_{x/proj}$	β_{20}	β_{30}	$E_{x/proj}$	β_{22}	β_{32}	$E_{x/proj}$	E_x [75]
MF	0.21	0.00	4.89	0.21	0.00	8.53	-0.16	0.03	6.94	0.00	0.00	9.46	-
0^+	0.23	0.07	0.00	0.01	0.23	0.00	0.00	0.21	0.00	0.06	0.00	0.00	0.00
2^+	0.25	0.07	0.91	0.22	0.12	4.65	-0.15	0.09	3.41	0.00	0.10	3.06	1.75
4^+	0.26	0.07	2.31	0.25	0.11	5.94	0.24	0.10	4.70	0.00	0.09	4.59	2.75
3^-	-	-	-	0.03	0.24	4.90	0.00	0.22	4.00	0.01	0.03	4.98	1.90
1^-	-	-	-	0.21	0.22	7.09	0.20	0.20	5.95	0.13	0.00	6.13	4.07
RHIC [20]				0.062	0.202								

($-0.19, 0.00$), respectively. After symmetry projections, we find a single energy minimum at (β_{20}, β_{30}) = (0.01, 0.23) on the 0^+ PES. The symmetry restorations give a large energy correction $E_{proj} =$ 8.53 MeV. The projected 2^+ and 4^+ PESs have similar structures: they both exhibit energy minimum at (β_{20}, β_{30}) $\approx$ (0.2, 0.1). One may conjecture that these states together with another 0^+ state with similar deformations belong to a typical rotational band. To examine the existence of such 0^+ state, we also need further GCM calculations.

On the 3^- PES in Fig. 2(b), we find a single energy minimum at (β_{20}, β_{30}) = (0.03, 0.24) with $E_x(3^-) = 4.90$ MeV. In contrary to the 2^+ and 4^+ states, its shape is close to that of the 0^+ state. We also present the 1^- PES. We find that the 1^- and 3^- minima have very different shapes. The very small experimental $E_x(3^-) = 1.90$ MeV and the deformations of the states point out the 3^- state may be a octupole vibrational collectivity [29] and the 0^+ is the band head of octupole vibration instead of that of a nearly spherical band predicted by the MCSM calculations [76].

Doctopic: Theory
JID:PLB   AID:137896 /SCO

ARTICLE IN PRESS

[m5G; v1.335] P.5 (1-7)

Y.-T. Rong, X.-Y. Wu, B.-N. Lu et al.

Physics Letters B ••• (••••) ••••••

Fig. 3. Comparison of the experimental low-spin ^{96}Zr levels with the results of (a) $K\!\!\!/\pi$, (b) $K\!\!\!/\pi$ and (c) $K\!\!\!/\pi$+PNP(δ) and (d) $K\!\!\!/\pi$ calculations. In $K\!\!\!/\pi$ case, the levels belong to γ band are not shown.

We also calculate $E(\beta_{20}, \beta_{30})$ in $K\!\!\!/\pi$ case with full particle-number projection (PNP) using the method developed in Ref. [65]. The results are shown in Fig. 2(c). Note that in these calculations we used different parameter settings compared to the other columns, such as the dimension of the basis space, the pairing force (in (c) we used a δ-pairing force, while in the other columns we used a separable pairing force) and the particle-number corrections (in (c) we performed an exact particle-number projection, while in the other columns we used the approximate ansatz Eq. (8)). For all J^π states with the same symmetries imposed, the PESs are qualitatively similar. The only noticeable difference is that the approximate scheme in (b) gives prolate minima for mean-field and 2^+ projected PESs, while the exact PNP method in (c) finds oblate minima on these PESs. The reason is that the PES of this nucleus is γ-soft and both axial-symmetric minima are nearly degenerate. A slight difference in the parameters can reverse the order of them. Thus, for more precise calculations the GCM must be included to mix the shapes.

In Fig. 2(d) we show the energy $E(\beta_{22}, \beta_{32})$ of mean-field state and the states with projections onto different spin-parity as a function of (β_{22}, β_{32}), while (β_{20}, β_{30}) are fixed to the values corresponding to energy minima in Fig. 2(b). For mean-field PES, the energy minimum is located at $(\beta_{22}, \beta_{32}) = (0.0, 0.0)$, indicating that the non-axial deformations are not favored, consistent with the prediction of the RHB theory [5], the HFB theories with Gogny interaction [46] and Skyrme interactions [6]. In contrast, after projection onto spin-parity $J^\pi = 0^+$, the energy minimum shifts to the deformations $(\beta_{20}, \beta_{22}, \beta_{30}, \beta_{32}) = (0.01, 0.06, 0.23, 0.00)$. However, the projected 0^+ PES is soft against (β_{22}, β_{32}) deformations. One may expect large shape fluctuations, the consideration of which is beyond the scope of this work. Nevertheless, our results show nontrivial contribution from both triaxial β_{22} and tetrahedral β_{32} deformations, which is consistent with the finding in Refs. [43,76] and the RHIC experiment [77]. Of course, this argument is based on the assumption that the location of the energy minimum in (β_{20}, β_{30}) plane does not move when varying (β_{22}, β_{32}). A more solid conclusion should be made based on the result of calculation for the states within the whole $(\beta_{20}, \beta_{22}, \beta_{30}, \beta_{32})$ deformation space, which is too expensive to be carried out in this work. Similarly, the above argument would also apply to all excited levels.

Next we examine the calculated energy levels and transition amplitudes. In Fig. 3, the calculated low-lying excitation energies, defined in Eq. (11), are shown and compared with the experimental data [75]. The $E_x(2^+)$ with $K\!\!\!/\pi$ symmetry is lower than the experimental value but the situation is opposite with $K\!\!\!/\pi$ case. The excitation energies extracted from full PNP calculations are larger than the experimental values by about 2 MeV, lower than the
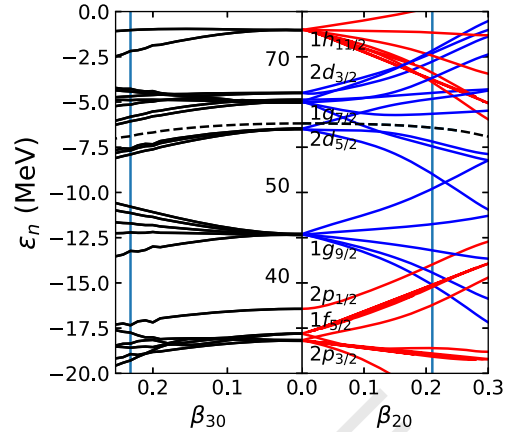
Fig. 4. Single-neutron levels of ^{96}Zr as functions of pure β_{20} (right half) and β_{30} (left half) deformations. The vertical lines on right and left halves correspond to global minima on the mean-field and 0^+ PESs in Fig. 2(b), respectively. The principal, orbital, and angular momentum quantum numbers nlj for spherical symmetry are presented. The dashed line denotes the Fermi level.

case with particle-number restriction for about 1 MeV. By breaking the axial symmetry, the energy levels 2^+, 4^+ and 1^- in $K\!\!\!/\pi$ calculations are lowered compared with the results in the $K\!\!\!/\pi$ calculations. Conversely, the 3^- energy is almost unaffected by the triaxial deformations. These level schemes are qualitatively similar to that from MCSM calculations [29].

In the current framework, the electric multipole transitions are calculated between states that are projected out with the same deformations. In other words, the shift of the nuclear shapes with spin is neglected. Under this approximation, we calculate the $B(E3; 3^- \rightarrow 0^+)$ using the symmetry-projected wave functions with intrinsic deformations $(\beta_{20}, \beta_{30}) = (0.01, 0.23)$, corresponding to the energy minimum of 0^+ state labeled with $K\!\!\!/\pi$. The result is 20.68×10^3 e^2 fm^6, which is comparable to the recent experimental value of $23(2) \times 10^3$ e^2 fm^6 [29]. Considering the fact that the energy minimum of the 3^- state coincidents with that of the 0^+ state, as shown in Fig. 2(b), it is reasonable to compare this calculated value with the data. From the energy spectrum, the lowest 3^- state probably belongs to an octupole vibration band, the proper description of which requires the inclusion of the shape mixing. It is beyond the current framework. However, it is interesting to note that the $B(E3)$ is in surprisingly good agreement with experimental data.

We also calculate the mean-field and projected PESs with DD-PC1 [78] and PC-F1 [56] parameter sets. The results are qualitatively the same as those we present here.

Microscopically, the emergence of octupole collectivity stems from the specific shell structures of single-particle levels around the Fermi level [1,79]. In Fig. 4 we plot the mean-field single-neutron levels of ^{96}Zr as functions of β_{20} (β_{30}) deformation. The single-proton levels below and around $Z = 40$ are qualitatively similar and not shown here. For the spherical shape $\beta_{20,30} = 0$, the neutron Fermi level lies between the $2d_{5/2}$ and $1g_{7/2}$ shells. In the left half of Fig. 4, we present the dependence of the single-neutron levels on pure β_{30} deformation. We see that the energy splittings caused by non-zero β_{30} are small, and the spherical gaps at $N = 40$, 50, and 70 are still remarkable. In the right half of Fig. 4, we show the splitting of the neutron energy levels due to a pure β_{20} deformation. Here the $1h_{11/2}$ state lying above the Fermi level splits into six levels. Thus, neutrons have the possibilities to occupy the $1h_{11/2}$ orbital with considerable amplitude, leading to strong octupole coupling with the orbital $2d_{5/2}$. As for single-proton energy levels, the $2p_{3/2}$ and $1f_{5/2}$ are the two states coupled via pure β_{20} deformation while the $1g_{9/2}$ and $2p_{3/2}$ can be coupled

Doctopic: Theory

ARTICLE IN PRESS

JID:PLB AID:137896 /SCO

[m5G; v1.335] P.6 (1-7)

Y.-T. Rong, X.-Y. Wu, B.-N. Lu et al.

Physics Letters B ••• (••••) ••••••

via pure β_{30} correlation. The energy splitting for non-zero β_{30} is again small compared with that for non-zero β_{20}, resulting in a large shell gap around the proton Fermi surface. For non-zero β_{20}, some proton levels from the $1g_{9/2}$ and $2p_{3/2}$ states are close to each other near the Fermi surface. Thus, the octupole deformation in ^{96}Zr is dominated by the proton levels $2p_{3/2} \rightarrow 1g_{9/2}$ and neutron levels $2d_{5/2} \rightarrow 1h_{11/2}$.

4. Summary

The competitions of various shell structures near $A \simeq 100$ create complex structures on the potential energy surfaces (PESs) of Zr isotopes. In particular, it was found that both triaxial and octupole deformations play important roles in ^{96}Zr, which presents a great challenge for calculations based on microscopic theories. Recently we implement a unified framework called p-MDCRHB model to calculate the potential energy surfaces with various symmetries. In this model both axial and reflection symmetries can be broken in the mean-field level and restored by projection-after-variation methods. Various symmetries can be imposed to speed up the calculations. With this model, we show that the PESs of ^{96}Zr have strong dependence on the angular momentum and parity. Most mean-field and projected PESs are soft for triaxial deformation β_{22} and tetrahedral deformation β_{32}. We also extract the energy levels at the global minima on each projected PES and compare them with the experiments. Our results suggest that both triaxial and octupole degrees of freedom are essential elements for precisely describing the structure of the ^{96}Zr nucleus. A more solid conclusion cannot be made before the full symmetry-restored GCM calculation with the mixing of all types of deformed configurations is carried out. Work along this direction is in progress.

Declaration of competing interest

The authors declare that they have no known competing financial interests or personal relationships that could have appeared to influence the work reported in this paper.

Data availability

Data will be made available on request.

References

[1] P.A. Butler, W. Nazarewicz, Intrinsic reflection asymmetry in atomic nuclei, Rev. Mod. Phys. 68 (1996) 349–421.

[2] P.A. Butler, Pear-shaped atomic nuclei, Proc. R. Soc. A 476 (2020) 20200202.

[3] P. Möller, R. Bengtsson, B. Carlsson, P. Olivius, T. Ichikawa, H. Sagawa, A. Iwamoto, Axial and reflection asymmetry of the nuclear ground state, At. Data Nucl. Data Tables 94 (5) (2008) 758–780.

[4] L.M. Robledo, G.F. Bertsch, Global systematics of octupole excitations in even-even nuclei, Phys. Rev. C 84 (2011) 054302.

[5] S.E. Agbemava, A.V. Afanasjev, P. Ring, Octupole deformation in the ground states of even-even nuclei: a global analysis within the covariant density functional theory, Phys. Rev. C 93 (2016) 044304.

[6] Y. Cao, S.E. Agbemava, A.V. Afanasjev, W. Nazarewicz, E. Olsen, Landscape of pear-shaped even-even nuclei, Phys. Rev. C 102 (2020) 024311.

[7] L.P. Gaffney, P.A. Butler, M. Scheck, A.B. Hayes, F. Wenander, M. Albers, B. Bastin, C. Bauer, A. Blazhev, S. Bᶜonig, N. Bree, J. Cederkᶜall, T. Chupp, D. Cline, T.E. Cocolios, T. Davinson, H. De Witte, J. Diriken, T. Grahn, A. Herzan, M. Huyse, D.G. Jenkins, D.T. Joss, N. Kesteloot, J. Konki, M. Kowalczyk, T. Kröll, E. Kwan, R. Lutter, K. Moschner, P. Napiorkowski, J. Pakarinen, M. Pfeiffer, D. Radeck, P. Reiter, K. Reynders, S.V. Rigby, L.M. Robledo, M. Rudigier, S. Sambi, M. Seidlitz, B. Siebeck, T. Stora, P. Thoele, P. Van Duppen, M.J. Vermeulen, M. von Schmid, D. Voulot, N. Warr, K. Wimmer, K. Wrzosek-Lipska, C.Y. Wu, M. Zielinska, Studies of pear-shaped nuclei using accelerated radioactive beams, Nature 497 (2013) 199.

[8] B. Bucher, S. Zhu, C.Y. Wu, R.V.F. Janssens, D. Cline, A.B. Hayes, M. Albers, A.D. Ayangeakaa, P.A. Butler, C.M. Campbell, M.P. Carpenter, C.J. Chiara, J.A. Clark, H.L. Crawford, M. Cromaz, H.M. David, C. Dickerson, E.T. Gregor, J. Harker, C.R. Hoffman, B.P. Kay, F.G. Kondev, A. Korichi, T. Lauritsen, A.O. Macchiavelli, R.C. Pardo, A. Richard, M.A. Riley, G. Savard, M. Scheck, D. Seweryniak, M.K. Smith, R. Vondrasek, A. Wiens, Direct evidence of octupole deformation in neutron-rich ^{144}Ba, Phys. Rev. Lett. 116 (2016) 112503.

[9] B. Bucher, S. Zhu, C.Y. Wu, R.V.F. Janssens, R.N. Bernard, L.M. Robledo, T.R. Rodríguez, D. Cline, A.B. Hayes, A.D. Ayangeakaa, M.Q. Buckner, C.M. Campbell, M.P. Carpenter, J.A. Clark, H.L. Crawford, H.M. David, C. Dickerson, J. Harker, C.R. Hoffman, B.P. Kay, F.G. Kondev, T. Lauritsen, A.O. Macchiavelli, R.C. Pardo, G. Savard, D. Seweryniak, R. Vondrasek, Direct evidence for octupole deformation in ^{146}Ba and the origin of large $E1$ moment variations in reflection-asymmetric nuclei, Phys. Rev. Lett. 118 (2017) 152504.

[10] M.M.R. Chishti, D. O'Donnell, G. Battaglia, M. Bowry, D.A. Jaroszynski, B.S.N. Singh, M. Scheck, P. Spagnoletti, J.F. Smith, Direct measurement of the intrinsic electric dipole moment in pear-shaped thorium-228, Nat. Phys. 16 (2020) 853.

[11] U. Heinz, A. Kuhlman, Anisotropic flow and jet quenching in ultrarelativistic U + U collisions, Phys. Rev. Lett. 94 (2005) 132301.

[12] Q. Shou, Y. Ma, P. Sorensen, A. Tang, F. Videbk, H. Wang, Parameterization of deformed nuclei for Glauber modeling in relativistic heavy ion collisions, Phys. Lett. B 749 (2015) 215–220.

[13] G. Giacalone, J. Jia, V. Somà, Accessing the shape of atomic nuclei with relativistic collisions of isobars, Phys. Rev. C 104 (2021) L041903.

[14] J. Jia, Shape of atomic nuclei in heavy ion collisions, Phys. Rev. C 105 (2022) 014905.

[15] G. Giacalone, J. Jia, C. Zhang, Impact of nuclear deformation on relativistic heavy-ion collisions: assessing consistency in nuclear physics across energy scales, Phys. Rev. Lett. 127 (2021) 242301.

[16] L. Adamczyk, J.K. Adkins, G. Agakishiev, et al., Azimuthal anisotropy in U + U and Au + Au collisions at RHIC, Phys. Rev. Lett. 115 (2015) 222301.

[17] S. Acharya, F. Acosta, D. Adamová, et al., Anisotropic flow in Xe-Xe collisions at $\sqrt{s_{NN}}$ = 5.44 TeV, Phys. Lett. B 784 (2018) 82–95.

[18] A.M. Sirunyan, A. Tumasyan, W. Adam, et al., Charged-particle angular correlations in XeXe collisions at $\sqrt{s_{NN}}$ = 5.44 TeV, Phys. Rev. C 100 (2019) 044902.

[19] G. Aad, B. Abbott, D.C. Abbott, et al., Measurement of the azimuthal anisotropy of charged-particle production in Xe + Xe collisions at $\sqrt{s_{NN}}$ = 5.44 TeV with the ATLAS detector, Phys. Rev. C 101 (2020) 024906.

[20] C. Zhang, J. Jia, Evidence of quadrupole and octupole deformations in ^{96}Zr + ^{96}Zr and ^{96}Ru + ^{96}Ru collisions at ultrarelativistic energies, Phys. Rev. Lett. 128 (2022) 022301.

[21] M.S. Abdallah, B.E. Aboona, J. Adam, et al., Search for the chiral magnetic effect with isobar collisions at $\sqrt{s_{NN}}$ = 200 Gev by the STAR collaboration at RHIC, arXiv:2109.00131, 2021.

[22] H. Mach, S. Ćwiok, W. Nazarewicz, B. Fogelberg, M. Moszyński, J. Winger, R.L. Gill, Strong octupole and dipole collectivity in ^{96}Zr: indication for octupole instability in the A = 100 mass region, Phys. Rev. C 42 (1990) R811–R814.

[23] H. Ohm, M. Liang, G. Molnár, S. Raman, K. Sistemich, W. Unkelbach, Strong harmonic $E3$ vibrations in ^{96}Zr, Phys. Lett. B 241 (4) (1990) 472–475.

[24] D. Hofer, M. Bisenberger, R. Hertenberger, H. Kader, H. Maier, E. Müller-Zanotti, P. Schiemenz, G. Graw, P. Maier-Komor, G. Molnár, W. Unkelbach, J. Hebenstreit, H. Ohm, D. Paul, P. von Rossen, M. Fujiwara, Direct and multiple excitations in ^{96}Zr from inelastic-scattering experiments, Nucl. Phys. A 551 (2) (1993) 173–209.

[25] D.J. Horen, R.L. Auble, G.R. Satchler, J.R. Beene, I.Y. Lee, C.Y. Wu, D. Cline, M. Devlin, R. Ibbotson, M.W. Simon, Lifetime of the 3^-_1 state and octupole collectivity in ^{96}Zr, Phys. Rev. C 48 (1993) R2131–R2134.

[26] S. Fayans, A. Platonov, G. Graw, D. Hofer, Microscopic description of low-lying one- and two-phonon states and application to ^{96}Zr, Nucl. Phys. A 577 (3) (1994) 557–584.

[27] O. Rosso, W. Unkelbach, G. Molnár, RPA and QRPA calculations for low-lying states in ^{96}Zr, Nucl. Phys. A 563 (1) (1993) 74–96.

[28] J. Skalski, P.-H. Heenen, P. Bonche, Shape coexistence and low-lying collective states in $A \approx$ 100 Zr nuclei, Nucl. Phys. A 559 (2) (1993) 221–238.

Doctopic: Theory

ARTICLE IN PRESS

JID:PLB AID:137896 /SCO

[m5G; v1.335] P.7 (1-7)

Y.-T. Rong, X.-Y. Wu, B.-N. Lu et al.

Physics Letters B ••• (••••) ••••••

[29] L. Iskra, R. Broda, R. Janssens, M. Carpenter, B. Fornal, T. Lauritsen, T. Otsuka, T. Togashi, Y. Tsunoda, W. Walters, S. Zhu, Revised $B(E3)$ transition rate and structure of the 3^- level in ^{96}Zr, Phys. Lett. B 788 (2019) 396–400.

[30] P. Möller, A. Sierk, T. Ichikawa, H. Sagawa, Nuclear ground-state masses and deformations: FRDM(2012), At. Data Nucl. Data Tables 109–110 (2016) 1–204.

[31] J. Yao, J. Meng, Y. Niu, P. Ring, Beyond-mean-field approaches for nuclear neutrinoless double beta decay in the standard mechanism, Prog. Part. Nucl. Phys. (2022) 103965.

[32] M. Bender, P.-H. Heenen, P.-G. Reinhard, Self-consistent mean-field models for nuclear structure, Rev. Mod. Phys. 75 (2003) 121.

[33] T. Nikšić, D. Vretenar, P. Ring, Relativistic nuclear energy density functionals: mean-field and beyond, Prog. Part. Nucl. Phys. 66 (2011) 519.

[34] J.L. Egido, State-of-the-art of beyond mean field theories with nuclear density functionals, Phys. Scr. 91 (2016) 073003.

[35] L.M. Robledo, T.R. Rodríguez, R.R. Rodríguez-Guzmán, Mean field and beyond description of nuclear structure with the gogny force: a review, J. Phys. G, Nucl. Part. Phys. 46 (1) (2018) 013001.

[36] J.A. Sheikh, J.J. Dobaczewski, P. Ring, L.M. Robledo, C. Yannouleas, Symmetry restoration in mean-field approaches, J. Phys. G, Nucl. Part. Phys. 48 (2021) 123001.

[37] X.-X. Sun, S.-G. Zhou, Rotating deformed halo nuclei and shape decoupling effects, Sci. Bull. 66 (20) (2021) 2072–2078.

[38] Y.S. Chen, Z.C. Gao, Reflection asymmetric shell model for octupole-deformed nuclei, Phys. Rev. C 63 (2000) 014314.

[39] J.M. Yao, E.F. Zhou, Z.P. Li, Beyond relativistic mean-field approach for nuclear octupole excitations, Phys. Rev. C 92 (2015) 041304.

[40] E. Zhou, J. Yao, Z. Li, J. Meng, P. Ring, Anatomy of molecular structures in ^{20}Ne, Phys. Lett. B 753 (2016) 227–231.

[41] J. Egido, L. Robledo, Parity-projected calculations on octupole deformed nuclei, Nucl. Phys. A 524 (1) (1991) 65–87.

[42] R.N. Bernard, L.M. Robledo, T.R. Rodríguez, Octupole correlations in the ^{144}Ba nucleus described with symmetry-conserving configuration-mixing calculations, Phys. Rev. C 93 (2016) 061302.

[43] S. Tagami, Y.R. Shimizu, J. Dudek, Tetrahedral symmetry in Zr nuclei: calculations of low-energy excitations with Gogny interaction, J. Phys. G, Nucl. Part. Phys. 42 (2015) 015106.

[44] X. Wang, G. Dong, Z. Gao, Y. Chen, C. Shen, Tetrahedral symmetry in the ground state of ^{16}O, Phys. Lett. B 790 (2019) 498–501.

[45] R. Rodríguez-Guzmán, L.M. Robledo, Microscopic description of quadrupole-octupole coupling in neutron-rich actinides and superheavy nuclei with the Gogny-D1M energy density functional, Phys. Rev. C 103 (2021) 044301.

[46] L.M. Robledo, Enhancement of octupole strength in near spherical nuclei, Eur. Phys. J. A 52 (2016) 300.

[47] Z. Li, B. Song, J. Yao, D. Vretenar, J. Meng, Simultaneous quadrupole and octupole shape phase transitions in Thorium, Phys. Lett. B 726 (4) (2013) 866–869.

[48] S.Y. Xia, H. Tao, Y. Lu, Z.P. Li, T. Nikšić, D. Vretenar, Spectroscopy of reflection-asymmetric nuclei with relativistic energy density functionals, Phys. Rev. C 96 (2017) 054303.

[49] K. Nomura, R. Rodríguez-Guzmán, L.M. Robledo, J.E. García-Ramos, N.C. Hernández, Evolution of octupole deformation and collectivity in neutron-rich lanthanides, Phys. Rev. C 104 (2021) 044324.

[50] K. Zberecki, P. Magierski, P.-H. Heenen, N. Schunck, Tetrahedral correlations in ^{80}Zr and ^{98}Zr, Phys. Rev. C 74 (2006) 051302(R).

[51] K. Zberecki, P.-H. Heenen, P. Magierski, Nuclear tetrahedral configurations at spin zero, Phys. Rev. C 79 (2009) 014319.

[52] B.-N. Lu, J. Zhao, E.-G. Zhao, S.-G. Zhou, Multidimensionally-constrained relativistic mean-field models and potential-energy surfaces of actinide nuclei, Phys. Rev. C 89 (2014) 014323.

[53] S.-G. Zhou, Multidimensionally constrained covariant density functional theories-nuclear shapes and potential energy surfaces, Phys. Scr. 91 (2016) 063008.

[54] K. Wang, B. Lu, Angular momentum and parity projected multidimensionally constrained relativistic Hartree-Bogoliubov model, Commun. Theor. Phys. 74 (1) (2022) 015303.

[55] B.A. Nikolaus, T. Hoch, D.G. Madland, Nuclear ground state properties in a relativistic point coupling model, Phys. Rev. C 46 (1992) 1757.

[56] T. Bürvenich, D.G. Madland, J.A. Maruhn, P.-G. Reinhard, Nuclear ground state observables and QCD scaling in a refined relativistic point coupling model, Phys. Rev. C 65 (2002) 044308.

[57] P. Ring, Relativistic mean field theory in finite nuclei, Prog. Part. Nucl. Phys. 37 (1996) 193.

[58] H. Kucharek, P. Ring, Relativistic field theory of superfluidity in nuclei, Z. Phys. A 339 (1991) 23.

[59] P.W. Zhao, Z.P. Li, J.M. Yao, J. Meng, New parametrization for the nuclear covariant energy density functional with a point-coupling interaction, Phys. Rev. C 82 (2010) 054319.

[60] Y. Tian, Z.-Y. Ma, A separable pairing force in nuclear matter, Chin. Phys. Lett. 23 (12) (2006) 3226–3229.

[61] Y. Tian, Z.Y. Ma, P. Ring, A finite range pairing force for density functional theory in superfluid nuclei, Phys. Lett. B 676 (2009) 44.

[62] J. Zhao, B.-N. Lu, E.-G. Zhao, S.-G. Zhou, Tetrahedral shapes of neutron-rich Zr isotopes from a multidimensionally constrained relativistic Hartree-Bogoliubov model, Phys. Rev. C 95 (2017) 014320.

[63] J.M. Yao, J. Meng, P. Ring, D. Vretenar, Configuration mixing of angular-momentum-projected triaxial relativistic mean-field wave functions, Phys. Rev. C 81 (2010) 044311.

[64] P. Ring, P. Schuck, The Nuclear Many-Body Problem, Springer-Verlag Berlin Heidelberg, 1980.

[65] J.M. Yao, J. Meng, P. Ring, D.P. Arteaga, Three-dimensional angular momentum projection in relativistic mean-field theory, Phys. Rev. C 79 (2009) 044312.

[66] M. Anguiano, J. Egido, L. Robledo, Particle number projection with effective forces, Nucl. Phys. A 696 (3) (2001) 467–493.

[67] N. Tajima, H. Flocard, P. Bonche, J. Dobaczewski, P.-H. Heenen, Generator coordinate kernels between zero- and two-quasiparticle BCS states, Nucl. Phys. A 542 (3) (1992) 355–367.

[68] M. Bender, T. Duguet, D. Lacroix, Particle-number restoration within the energy density functional formalism, Phys. Rev. C 79 (2009) 044319.

[69] T. Duguet, M. Bender, K. Bennaceur, D. Lacroix, T. Lesinski, Particle-number restoration within the energy density functional formalism: nonviability of terms depending on noninteger powers of the density matrices, Phys. Rev. C 79 (2009) 044320.

[70] J. Dobaczewski, M.V. Stoitsov, W. Nazarewicz, P.-G. Reinhard, Particle-number projection and the density functional theory, Phys. Rev. C 76 (2007) 054315.

[71] D. Lacroix, T. Duguet, M. Bender, Configuration mixing within the energy density functional formalism: removing spurious contributions from nondiagonal energy kernels, Phys. Rev. C 79 (2009) 044318.

[72] F. Dönau, Canonical form of transition matrix elements, Phys. Rev. C 58 (1998) 872–877.

[73] D. Almehed, S. Frauendorf, F. Dönau, Pairing correlations in high-K bands, Phys. Rev. C 63 (2001) 044311.

[74] M. Wang, W. Huang, F. Kondev, G. Audi, S. Naimi, The AME 2020 atomic mass evaluation (II). Tables, graphs and references, Chin. Phys. C 45 (3) (2021) 030003.

[75] B.N.L. National Nuclear Data Center, Nudat (Nuclear Structure and Decay Data), 2008.

[76] C. Kremer, S. Aslanidou, S. Bassauer, M. Hilcker, A. Krugmann, P. von Neumann-Cosel, T. Otsuka, N. Pietralla, V.Y. Ponomarev, N. Shimizu, M. Singer, G. Steinhilber, T. Togashi, Y. Tsunoda, V. Werner, M. Zweidinger, First measurement of collectivity of coexisting shapes based on type II shell evolution: the case of ^{96}Zr, Phys. Rev. Lett. 117 (2016) 172503.

[77] J. Jia, Probing triaxial deformation of atomic nuclei in high-energy heavy ion collisions, Phys. Rev. C 105 (2022) 044905.

[78] T. Nikšić, D. Vretenar, P. Ring, Relativistic nuclear energy density functionals: adjusting parameters to binding energies, Phys. Rev. C 78 (2008) 034318.

[79] H. Jahn, E. Teller, Stability of polyatomic molecules in degenerate electronic states: I–Orbital degeneracy, Proc. R. Soc. A, Math. Phys. Eng. Sci. 161 (1937) 220.